Ceramics International xxx (xxxx) xxx–xxx

Contents lists available at ScienceDirect

Ceramics International

journal homepage: www.elsevier.com/locate/ceramint

Near-net shaping of silicon nitride via aqueous room-temperature injection molding and pressureless sintering

Lisa M. Rueschhoff, Rodney W. Trice*, Jeffrey P. Youngblood

School of Materials Engineering, Purdue University, West Lafayette, Indiana 47907, USA

ARTICLE INFO

Keywords:
(A) Suspensions
Injection molding and (D) Si_3N
Mechanical properties

ABSTRACT

Silicon nitride (Si_3N_4) is of interest because of its high inherent fracture toughness due to interlocking and elongated β-Si_3N_4 grains, but it is difficult to economically produce into near-net and complex shapes. In this study, the difficulties were overcome with the use of a novel injection molding process where highly loaded (up to 45 vol%) suspensions were loaded into a syringe and injected at a controlled rate into a mold of a desired shape. The suspensions have carefully tailored yield-pseudoplastic rheology such that they can be injection molded at room temperature and low pressures (< 150 kPa). Four suspensions were studied; two different commercially available concrete water-reducing admixtures (WRAs) were used as dispersants with and without a polymer binder (Polyvinylprolidone, PVP) added for rheological modification and improved green body strength. Test bars formed via this process were sintered to high densities (up to 97% TD) without the use of external pressure, and had complete conversion to the desirable β-Si_3N_4 phase with high flexural strengths up to 700 MPa. The specimen sets with the smallest average pore size on the fracture surface (77 μm) had the highest average flexural strengths of 573 MPa. The hardness of all specimens was approximately 16 GPa. The ease and low cost of processing of these water-based suspensions, and the robust mechanical properties reported, demonstrate this as a viable process for the economical and environmentally friendly production of Si_3N_4 parts.

1. Introduction

Of special interest is the fracture toughness of Si_3N_4, which has been reported to be nearly twice that of any other monolithic ceramic due to unique interlocking elongated β-Si_3N_4 grains that promote crack deflection and crack bridging in the material [1–3]. Si_3N_4 is an attractive material for high-temperature turbine engine parts, as well as other numerous structural applications, based on high flexural strength and hardness, superior wear resistance, and substantial creep resistance up to 1350 °C [4]. However, the use of Si_3N_4 in these high-temperature, high-stress applications is severely limited by production costs and the difficulty of forming the necessary complex shapes [5,6]. Due to these issues, the commercial use of Si_3N_4 has been limited to simple shapes like ball bearings and cutting tools produced via hot pressing [5,7]. The use of a more cost-effective and near-net shaping technique (one that does not require post forming processing), paired with pressureless sintering, can enable the expansion of this material into advanced technology areas including aerospace, automotive, and biomedical implants [8].

One method to overcome these typical problems associated with processing advanced ceramics is through a traditional powder injection molding (PIM) process [9]. This technique is based on mixing of ceramic powders with a polymer binder mixture to create a feedstock, which is then injected at high pressures and temperatures due to the high feedstock viscosity [9]. PIM has been applied successfully to many advanced ceramic systems, including silicon nitride, and is a promising ceramic processing method due to the ability to produce near-net and complex shapes with high precision at high production rates [9–12]. Some major problems have been identified with this process, though, including extended binder burnout processes (large parts can have cycles up to a week in length) which lead to slumping and crack formation [9,13,14]. Thicker cross sections (~1 cm) often require binder burnout cycles of 20 h to one week in length, making it difficult, if not impossible, to use traditional PIM to produce parts with thick cross sections [9,14]. The long binder burn-out times, along with high tooling costs, still limit the commercial use of PIM for ceramic production [14]. Binder burnout issues can be mitigated through significant decreases in polymer additives used, while tooling costs can be reduced through reducing the pressures and temperatures needed for molding.

Silicon nitride has been produced through a modified PIM approach from Millán et al. with use of aqueous Si_3N_4 suspensions and

* Correspondence to: 701 W. Stadium Ave, West Lafayette, IN 47907, USA.
E-mail address: rtrice@purdue.edu (R.W. Trice).

http://dx.doi.org/10.1016/j.ceramint.2017.05.097
Received 12 March 2017; Received in revised form 12 May 2017; Accepted 13 May 2017

agarose added as a gelling agent [15]. Rheological tailoring, through the addition of strong bases and temperature modifications, of the ~40 vol% solids loading suspensions was used to decrease the pressure and temperatures needed during injection molding to 0.4 MPa and 60 – 65 °C, respectively [15]. Expensive PIM tooling was still used for the forming experiments, and somewhat low densities (~90%TD) were obtained with no mechanical behavior reported [15].

This current work proposes the use of highly-loaded (up to 45 vol%) aqueous Si_3N_4 suspensions, along with a room-temperature and low-pressure injection molding process, as an alternate processing method to effectively and economically produce near-net shaped Si_3N_4 parts without the use of harsh cross-linking or curing agents or further chemical processes. Our previous research found a novel route of using comb-polymer water reducing admixtures (WRAs), commercially produced for the concrete industry, as a dispersant for Si_3N_4 powders in water [16]. These comb-polymers offer steric stabilization in the system through adsorption of the charged polyacrylic acid (PAA) based backbone of the polymer on the ceramic particle surface, while the uncharged polyethylene oxide (PEO) side chains extend into solution and repels other particles [16]. The suspensions have been well stabilized through these comb-polymer dispersants so no temperature increases or strong acids or bases are needed to lower their viscosity. These suspensions have yield-psuedoplastic flow behavior desirable for this process; they are highly shear thinning with flowable viscosities at room temperature and their characteristic yield stress helps a part retain shape after injection molding so that no gelation additives are needed.

Two comb-polymer WRA dispersants, ADVA CAST 575 and Glenium 7500, were identified as optimal and were explored along with suspensions containing Polyvinylprolidone (PVP), a non-toxic and water soluble linear polymer added for rheological tailoring and improved green body strength. These four suspensions (two dispersants, with and without polymer added) were used in this room-temperature and low-pressure injection molding process to identify suspensions which create the most dense and mechanically robust Si_3N_4 parts. The use of inexpensive and commercially available plastic syringes, along with rapidly produced polymer molds, makes this a more economical and environmentally friendly process that can be scaled for mass production. The low amount of polymer used (3–7.5 vol%), can help avoid defects that traditionally come with the long binder-burnout cycles needed in traditional PIM.

2. Experimental approach

2.1. Suspension preparation and characterization

Alpha silicon nitride powders (SNE-10, UBE Industries, Japan), with company specified d_{50} of 0.50 μm and specific surface area (SSA) of 9–13 m^2/g, were used in this study. Powders from lot number A136828 were used with a SSA of 10.6 m^2/g (As measured by UBE). All experiments utilized 5 wt% aluminum oxide (Al_2O_3) and 5 wt% yttrium oxide (Y_2O_3) as sintering aids as they have been proven to facilitate liquid phase sintering in Si_3N_4 at low temperature (< 1800 °C) to achieve high densities (> 95%TD) [17–21]. The Al_2O_3 had an average particle size of 0.50 μm and specific surface area of 7–12 m^2/g (grade A-16 SG, Almatis, Leetsdale, PA), while the Y_2O_3 (Sigma Aldrich, St. Louis, MO) had a company specified d_{50} of 2–10 μm. The sintering aids were mixed with Si_3N_4 powders, without milling media, using a dual-centrifugal speed mixer (DAC 400, Flacktek Inc, Landrum, SC) for 2 min at 850 RPM to ensure uniformity. This low rate was used to avoid particle size or morphology change during mixing.

Table 1 shows the name and composition of the suspensions used in this study. The commercially available concrete water reducing admixtures come as aqueous solution and were ADVA CAST 575 (W.R. Grace, Columbia, MD) and Glenium 7500 (BASF, Ludwigshafen, Germany) and will henceforth be referred to as dispersants. Our previous study using these dispersants found optimal loadings of 1.9 mg/m^2 and 2.9 mg/m^2 (with respect to the ceramic loading) for ADVA 575 and Glenium 7500, respectively [16]. PVP (1-ethenyl-2-pyrrolidinone homopolymer, 55,000 g/mol, Sigma-Aldrich, St. Louis, MO) was added in some suspensions for green body strength and rheological modification, and it will be referred to as a binder. Si_3N_4 suspensions were fabricated by mixing reverse osmosis (RO) water with the appropriate dispersant and binder content, followed by slowly mixing in the Si_3N_4 and sintering aid mixture in 10 g increments. The previously mentioned dual centrifugal mixer was used to thoroughly mix these highly-loaded suspensions. Mixing increments were done for 1–3 min starting at 800 RPM and increasing to up to 2000 RPM with increasing solids loading, with total mixing time taking less than 1 h. Suspensions were used for either rheology testing or injection molding approximately 24 h after mixing.

Rheological properties of the suspensions were determined using a Malvern Bohlin Gemini HR rheometer (Malvern Instruments Ltd, Worcestershire, UK) with a 25 mm cup and bob geometry fixture and a gap of 150 μm. Approximately 13 mL of each suspension was used for each test, and a water trap was used to prevent premature drying of the suspension during testing. Each suspension was pre-sheared for 60 s at a shear rate of 1 s^{-1} to ensure a uniform shear history. A shear rate from 0.005 to 30 s^{-1} (on a logarithmic scale) was applied to measure the low-shear viscosity and shear stress of the samples. The shear rate applied to the suspensions during room-temperature injection molding was estimated to be 1 s^{-1}, considering a syringe diameter of 8 mm and a compression rate of 5 mm/min applied by the MTS while forming. This approximate shear rate is much lower than the rates experienced during traditional PIM, typically on the order of 100–1000 s^{-1} and sometimes reaching 15,000 s^{-1} [11,15,22,23].

The shear stress measured as a function of applied shear rate for each sample was fitted to the Herschel-Bulkley model for yield-pseudoplastic fluids [24], using a method of least squares, defined as:

$$\sigma = \sigma_y + k\dot{\gamma}^n$$

where σ is the measured shear stress, σ_y is the yield stress, k is the consistency index, $\dot{\gamma}$ is the applied shear rate, and n is the flow index (with values ranging from 0 to 1). A given material is considered shear-thinning if the flow index is less than 1 [25]. Materials with flow index values greater than 1 are considered shear thickening and have

Table 1
Composition and rheological behavior of Si_3N_4 suspensions used in injection molding experiments.

				Herschel-Bulkley Curve-fit Parameters		
Sample Name	**Dispersant content (vol%) [mg/m²]**	**PVP content (vol%)**	**Viscosity at 1 s^{-1} (Pa-s)[b]**	**Yield Stress, σ_y (Pa)**	**k (Pa.s^n)**	**n**
A575	3 [1.9]	0	43.6	24.0	17.3	0.54
A575-PVP[1]	3 [1.9]	2.5	166.6	128.7	35.1	0.50
G7500	5 [2.9]	0	66.7	54.5	11.8	0.69
G7500-PVP	5 [2.9]	2.5	122.0	101.7	17.9	0.77

[1] Critical shear rate of dilatant behavior ~ 4 s^{-1}.
[b] Estimated shear rate during injection molding.

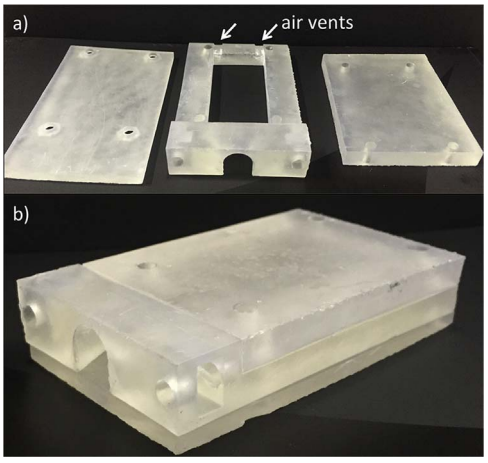

Fig. 1. a) Disassembled 3-piece mold for the injection molding process and b) assembled view.

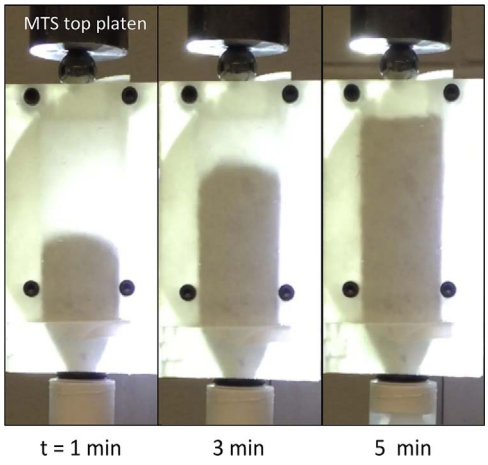

Fig. 2. Time lapse showing a Si_3N_4 suspension as it is injected into the mold shown in Fig. 1.

difficulties with flow and the binder separating from the ceramic powder, making them undesirable for processing [26].

2.2. Room-temperature injection molding

Due to the low pressures and temperatures during molding, it was possible to use inexpensive polymer tooling. A three-piece mold, shown in Fig. 1, used in the injection molding process was created using a Form 1+(Formlabs, Somerville, MA) stereolithography (SLA) 3D printer. Fig. 1a) shows a disassembled view of the bottom, middle, and top piece of the mold (from left to right). The middle section of the mold is equipped with twin 4 mm slits at the end (annotated in the figure) to allow air and excess material to escape during mold filling. The dimensions of this mold were designed to produce a green body rectangular billet 60 mm×25 mm×7 mm. Fig. 1b) shows the mold parts assembled with an opening port for the syringe. Wetted ashless filter paper (Grade 40, Whatman, UK) was used inside the top and bottom pieces of the mold to facilitate drying and part removal.

The Si_3N_4 suspensions were loaded into a 20 cc syringe with an inner tip diameter of 8 mm. The filled syringe was covered with parafilm and was mixed for 1 min at 850 RPM using a syringe holder in the Flacktek SpeedMixer in an attempt to homogenize the suspension and remove porosity that may have been introduced during filling. The syringe was inserted into the mold opening with a rubber O-ring, with the base of the syringe plunger and the top of the mold placed between two stainless steel platens in an MTS load frame (MTS Insight 100 load frame, MTS Systems Corporation, Eden Prairie, MN). To help circumvent closed pore formation due to air bubbles developing within the suspension during filling, a VM-25 miniature air piston vibrator (Cleveland Vibrator Co., Cleveland, OH) that had a frequency of 16,000 vibrations per minute at 0.55 MPa was secured to the top of the mold cavity during mold filling.

Fig. 2 shows the Si_3N_4 suspension filling the mold at an MTS crosshead speed of 5 mm/min, taking approximately 5 min to fill the entire mold. It should be noted that this slow rate was chosen for this study to ensure a low shear rate due to the rheological behavior of the A575 suspension (discussed further in Section 3.1), but in general much faster speeds can be used in this process to shorten molding time. Once molded, the specimens were left to dry at room temperature. The four screws that hold together the three-piece mold were removed within 15 min, and the top piece of the mold was removed approximately 30 min after molding. The bottom mold piece was removed approximately 30 min later, giving a total de-molding time of approximately 1 h. The green strength of the specimens allowed for easy de-molding and machining. The triangle entry section of the mold (seen in Fig. 2) was cut off with a razor blade on all specimens in the green state.

2.3. Binder burnout and pressureless sintering

Once demolded and dried overnight, specimens underwent binder burnout in an Al_2O_3 crucible in a tube furnace with flowing air at a heating rate of 5 °C/min until 650 °C where it was held for 6 h. A previous study reported thermogravimetric analysis (TGA) results with these dispersants showing complete burn-out in both flowing oxygen and nitrogen atmospheres [16]. After binder burnout, the specimens were transferred to a rectangular boron nitride crucible (Stanford Advanced Materials, Irvine, CA) 50.8×50.8×101.6 mm with a powder bed composed of 50 wt% boron nitride (grade HCPH, Advanced Ceramic Corporation, Cleveland, OH) and 50 wt% Si_3N_4 + sintering aid mixture. This type of powder bed is typically used in Si_3N_4 pressureless sintering to reduce volatilization due to the creation of a local gas equilibrium immediately adjacent to the Si_3N_4 compact [19,27–29]. The billets were stood up length-wise on each edge of the crucible such that 4 billets could be sintered at once. The specimens were sintered in a Centorr Testor Furnace (Centorr Vacuum Industries, Nashua, NH) in a nitrogen atmosphere with less than 10^{-7} ppm O_2 (commercial nitrogen gas purified through a 2G-100-SS Centorr Gettering Furnace). A heating rate of 25 °C/min was used until a set point of 1750 °C where the specimens were held for 1 h with no external pressure applied.

2.4. Characterization

After sintering, each billet was planarized on both sides using a surface grinder and 12.7 mm wide diamond wheel (McMaster-Carr, Chicago, IL) through lowering 2 μm between passes until completely flat surfaces were achieved. Each billet was then cut into three rectangular bars (approximate size 3×4×45 mm) using a 0.90 mm thick diamond blade (McMaster-Carr, Chicago, IL). The bars were again planarized with the diamond wheel to achieve uniform height and width dimensions. The density of the test bars was measured using Archimedes' method (ASTM C373-14a), and the true density (%TD) of the specimens, 3.288 g/cm^3, was calculated using a rule-of-mixtures approach based on the volume amounts of added sintering aids. The densities used for Si_3N_4, Al_2O_3, and Y_2O_3 were 3.187 g/cm^3, 3.98 g/cm^3, and 5.03 g/cm^3, respectively [30,31].

Hardness of the mounted and polished bend bar fragments was measured with a microindenter (LM247, LECO, St. Joseph, MI) using a Vickers head set to a 500 N load and 13 s hold time. Ten indents (optically examined to comply to ASTM C1327-15 standard) were measured to obtain a mean and standard deviation for each sample set. X-ray diffraction (XRD, D8 Focus, Bruker, Madison, WI) of the sintered specimens was used to confirm conversion to the β-Si_3N_4 phase.

The flexural strength of the specimens was measured using an MTS machine and 3-point semi-articulated fixture with a crosshead speed of 0.5 mm/min. A minimum of 5 bars, based on ASTM C 1161-02c standard size B specimens (3×4×45 mm) with the long tensile edges chamfered, were tested for each suspension formulation. The Weibull modulus and characteristic strength were calculated in accordance with ASTM C1239-13 based on the flexural strength values of the specimens. After testing, bend bar fragments were mounted, polished, and etched using a dilute HF solution (10 wt%, Sigma-Aldrich, St. Louis, MO) for SEM (Philips XL-40, FEI, Hillsboro, OR) analysis of microstructure. Optical images of the bend bar fracture surfaces taken at 2x magnification, along with ImageJ software, was used to measure pore size on the fracture surface. Each pore on the fracture surface was manually measured using the oval shape and analyze particle function in ImageJ, with the average of each suspension set calculated as the average of all bend bar surface averages.

Since the fracture in this study occurs under Mode I conditions, the fracture toughness, K_{IC}, can be estimated using the following equation:

$$K_{IC} = Y\sigma_f\sqrt{c}$$

where: Y is the stress intensity shape factor, c is the crack size, σ_y and is the stress at fracture. In this study, the measured average pore size on the fracture size is set equal to 2c and the calculated average flexural strength is used as σ_f. The stress intensity shape factor is a dimensionless parameter that takes into account the shape of the crack and the loading conditions, and has been estimated as 1.3 for this study based on an equation derived by Newman and Raju [32]. Using this equation will give a general estimate of the fracture toughness in this study, with the assumption that the average pore size calculated is representative of the dimensions of the strength-limiting flaw.

A two-tailed t-test was used to confirm a statistical significance of measured parameters in this study. A homoscedastic t-test was performed for samples with equal variance, while a heteroscedastic t-test was used with samples with unequal variance. A Microsoft Excel function was used to calculate the t-test, and data sets were considered statistically significant when $p < 0.05$.

3. Results and discussion

3.1. Suspension characterization

The suspensions used in this study, along with their rheological behavior, are outlined in Table 1. All suspensions exhibited yield-psuedoplastic behavior desirable for the injection molding process. Extensive rheological examination and optimization of the A575 and G7500 suspensions was completed in a previous study [16]. The viscosity as a function of applied shear rate for all suspensions is shown in Fig. 3, with the estimated shear rate during forming (1 s^{-1}) marked with a dotted line. An inset image in Fig. 3 shows the shear stress as a function of shear rate flow curves. These flow curves were fit to the Herschel-Bulkley model (shown as solid lines in the graph with $R^2 > 0.98$), with fit parameters listed in Table 1. Between the two dispersants, the A575 suspension had both lower yield stress (24.0 Pa compared to 54.5 Pa) and viscosity (50 Pa-s compared to 75 Pa-s) at 1 s^{-1}. The yield stress of the suspensions is associated with flocculation in the system that is broken up at higher shear rates to initiate flow [33], so A575 appears to be more effective than G7500 in stabilizing the Si_3N_4 suspensions through decreasing the amount of flocs.

Adding 2.5 vol% PVP to the suspensions increased both the yield stress and viscosity of both dispersants, as reported in similar studies with adding PVP to alumina suspensions [34,35]. For A575-PVP, the yield stress increased by over 5 times to 128.7 Pa, and the viscosity nearly tripled to 190 Pa-s. This suspension transitioned to shear thickening (also known as dilatant) behavior at a critical shear rate of approximately 4 s^{-1}, as shown as a sharp increase in viscosity in Fig. 3. This transition to shear-thickening behavior is seen in many highly-loaded suspensions and is speculated to be caused by an order-disorder transition where particle "jamming" causes an increase in viscosity [36]. Though this behavior is undesirable for ceramic processing, it is not expected to affect forming since the transition happens at shear rates above those experienced during this injection molding process. The G7500-PVP suspension showed no shear-thickening behavior in the shear rates studied, but the addition of PVP caused the yield stress to nearly double to 101.7 Pa, while the viscosity increased slightly, only to 120 Pa-s. The increases in both yield stress and viscosity indicates that the addition of PVP into the systems increased the amount of particle flocculation, with the largest effect seen in the A575-PVP suspension. In the shear rate regime of forming (1 s^{-1}), all suspensions had viscosities less than 200 Pa-s and were flowable at room temperature. These viscosities are much lower than the ceramic polymer melts used in traditional PIM, which generally have viscosities greater than 1000 Pa-s and require high temperature and applied pressure to flow [13].

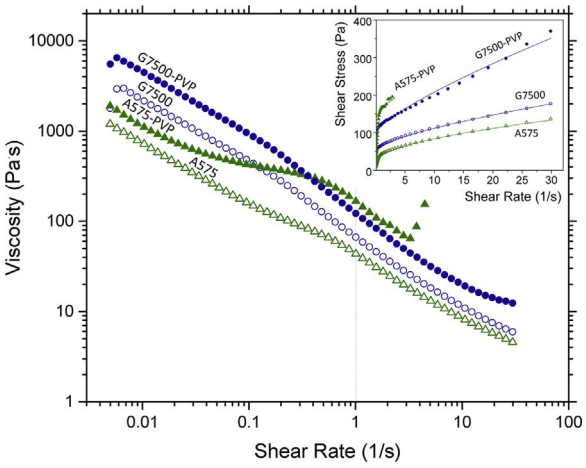

Fig. 3. Viscosity of the suspensions used in this study as a function of applied shear rate at room-temperature. The shear rate during injection molding, 1 s^{-1}, is marked with a dotted line. The inset graph shows the shear stress versus shear rate for the same suspensions, with solid lines showing the Herschel-Bulkley curve fit for each.

3.2. Injection molded specimen characterization

All suspensions were successfully used in the injection molding process to create green bodies. Fig. 4 shows two A575 billets, one in the green state (left) and the other after pressureless sintering (right). All specimens survived binder burnout without any cracks or other defects observed, a problem often encountered during the longer burnout process used to remove the higher amounts of binder used in traditional PIM [37]. In fact, this burnout cycle is nearly one third the time of other PIM processes where ~50 vol% binder was used [37].

The average bulk density of the sintered test bars is listed in Table 2 for each of the four suspension sets studied. The average density of the sample sets ranged from 94.0% to 95.2% TD, with some individual test bars as high as 97% TD. Specimens made from suspension A575 had the lowest average bulk density of 94.0%TD, which was statistically lower than those made from A575-PVP and G7500-PVP (confirmed using a two-tailed t-test with p=0.02), but similar to those from G7500 (p=0.09). While G7500 had the largest average bulk density of 95.2% TD, the values were statistically similar to the rest of the sample sets (p=0.09 to 0.57), likely due to the largest standard deviation in measured densities for the sample. In general, the suspension used in the injection molding process did not seem to have significantly affected the sintered density.

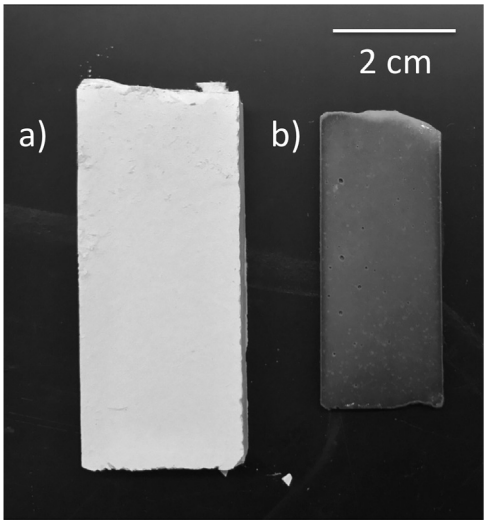

Fig. 4. Representative Si_3N_4 billets produced via injection molding a) in green state after drying at room temperature and another b) after binder burnout and pressureless sintering.

3.3. Microstructure and composition

The microstructure of a sintered and etched A575 specimen in shown in Fig. 5. In the image, elongated grey β–Si_3N_4 grains can be seen surrounded by a light intergranular glass phase. This microstructure is representative of all the specimens studied, with no grain size or morphology differences observed between specimen sets. There was also no observation of preferential orientation of the elongated grains due to the injection molding process during SEM analysis of the microstructure. The elongated β–Si_3N_4 grains from the micrograph in Fig. 5 have a nominal average aspect ratio of 6, as calculated from manual length and width measurements in ImageJ of 50 elongated grains. The average aspect ratio of elongated β-Si_3N_4 grains generally varies from 2 to 10 and depends on the sintering aids as well as sintering time and temperature [3]. Extensive work has been done to show that Si_3N_4 dissolves into a molten SiO_2-Y_2O_3-Al_2O_3 liquid that aid in densification and is quenched to a Y-Si-Al-O-N glass [38]. The amount of intergranular glass in this particular microstructure was calculated as 11.8% of the total area using ImageJ measurements through thresholding the image to isolate this intergranular phase. High-density regions are seen throughout the microstructure with some submicron pores and defects observed, which likely arose during sintering and preparation of mechanical specimens, respectively. Throughout the microstructures there was no large evidence of porosity due to incomplete sintering, therefore the 5–6% porosity calculated via density measurements is assumed to be from the forming process. XRD analysis (not shown) on sintered specimens from each suspension set showed prominent β-Si_3N_4 peaks at 2θ values of 27°, 34°, and 36° (based on JC-PDF #33–1160) and no α-Si_3N_4 peaks, confirming full conversion to the desirable β-Si_3N_4 high-temperature phase.

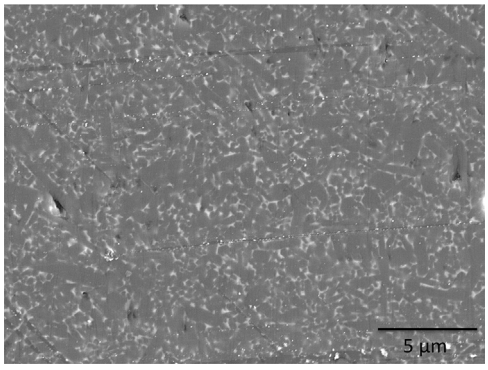

Fig. 5. A representative sintered and etched Si_3N_4 billet made via injection molding showing a typical microstructure of elongated β-Si_3N_4 grains (grey) in a glassy matrix (white).

3.4. Mechanical behavior

Values of the mechanical properties of the bend bars tested are listed in Table 2. There was no statistical significance between the Vickers hardness values for the four data sets, with an overall average between all samples of 15.7 ± 0.4 GPa. The hardness of Si_3N_4 depends on the type and amount of sintering aids used, but this value is similar to the hardness from other studies of pressureless sintering of Si_3N_4 which reported hardness from 12.4 to 16.7 GPa [27,39–41].

A SEM image of the fracture surface of a G7500 bend bar is shown in Fig. 6. This image was taken near the tensile surface of the bend bar and is representative of the fracture surfaces of all bend bars. All bend bars failed in the middle of the specimen (below the top bearing) and broke into two pieces with fracture surfaces perpendicular, or near perpendicular, to the main axis of the bend bar, indicating a lower energy failure. Elongated β-Si_3N_4 grain pullout can be observed on the fracture surface, and is pointed at in Fig. 6 with a white arrow. This type of feature is commonly found on sintered Si_3N_4 flexural strength bend bar specimens [42].

The average flexural strength for the four sample sets ranged from 342 to 573 MPa, with individual test bars as high as 695 MPa. The strength is quite consistent between sample sets as the standard deviation of each set was no greater than 18% of the average strength. For the suspensions dispersed with ADVA 575, there was a significant increase in the average flexural strength ($p \ll 0.05$) with the addition of PVP, from 341.5 to 536.8 MPa. Conversely, for the suspensions dispersed with Glenium 7500, there was a significant decrease in the average flexural strength ($p \ll 0.05$) with the addition of PVP, from 573.4 to 394.2 MPa.

Table 2
Mechanical behavior for sintered Si_3N_4 test bars produced via aqueous injection molding.

Suspension	Average Sintered Bulk Density (% TD)	Vickers Hardness (GPa)	Average Flexural Strength[a] (MPa)	Characteristic Strength, σ_0 (MPa)	90% Confidence Bounds for σ_0 (MPa)	Weibull Modulus, m	90% Confidence Bounds for m	Average Pore Size on Fracture Surface (µm)	Estimated Fracture Toughness, K_{IC} (MPa $m^{0.5}$)[b]
A575	94.0 ± 0.2	15.7 ± 0.1	341.5 ± 61.0	368.4	305.2–455.4	5.9	2.1–8.6	143.4 ± 41.0	3.76
A575-PVP	94.9 ± 0.9	15.7 ± 0.4	536.8 ± 48.1	566.5	534.6–601.6	11.9	6.3–16.4	90.5 ± 28.5	4.70
G7500	95.2 ± 1.4	15.5 ± 0.5	573.4 ± 63.9	603.1	555.8–657.3	10.1	4.7–14.3	76.9 ± 17.4	4.62
G7500-PVP	95.0 ± 0.6	15.9 ± 0.6	394.2 ± 52.7	420.6	364.9–493.9	7.76	2.8–11.4	124.2 ± 33.2	4.04

[a] Three-point bending.
[b] Calculated with the average flexural strength and the assumption that the average pore size on fracture surface =2c.

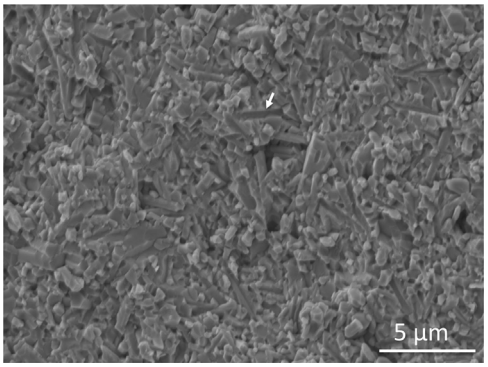

Fig. 6. A representative fracture surface on the tensile edge of a flexural test bar used in 3-point bending. An example of β-Si_3N_4 grain pullout is highlighted with a white arrow.

It can be difficult to compare strength values of Si_3N_4 in prior work due to the dependence on amount and type of sintering aid, which affects the resulting grain structure and intergranular phase chemistry, along with other processing parameters such as testing configuration and specimen size and density [43]. Because of these variables, a wide range of flexural strength values, ranging from 400 to 900 MPa, have been reported in literature for pressureless sintered Si_3N_4 [27,28,39–41,43,44]. Zeng et al. used a 45 vol% solid loading Si_3N_4 gelcasting slurry with similar sintering aids (6 wt% Y_2O_3, 2 wt% Al_2O_3) and pressureless sintering at 1780 °C to obtain specimens with 93.4% TD and 3-point bend flexural strength of approximately 350 MPa. Through increasing solids loading to 52 vol%, they reported an increase in both density and flexural strength to 97.8%TD and 687 MPa, respectively [28]. It is assumed that in the present study a similar improvement in mechanical properties is feasible with an increase in aqueous suspension solids loading.

The Weibull plots are shown in Fig. 7, with the Weibull modulus (m) and characteristic flexural strength (σ_0) calculated from the slope and intercept, respectively. The Weibull parameters, along with their 90% confidence bounds (calculated via equations from ASTM C1239-13 standard), are listed in Table 2. The relatively small number of test specimens used in this study results in a high uncertainty associated with the parameter estimates and is reflected in the larger spread in the confidence bounds. More specimens would be needed to have a more accurate calculation of these values and to achieve a tighter confidence bound for the variables. Therefore, in this study, the parameter estimates are meant to provide relative values at which to compare the flexural strength data scatter between the sample sets.

A575 had the lowest Weibull modulus of 5.9, corresponding to greater scatter in the flexural strength values. The G7500-PVP samples also had a lower Weibull modulus of 7.8, partially due to an outlying point of a higher flexural strength value of 490 MPa (the average for this set is 390 MPa). Upon examination of the fracture surface, the critical flaw for this sample was a subsurface pore, while the other samples in the set failed due to surface porosity. The difference in failure mode likely caused the large differences in strength and subsequent low Weibull modulus. A575-PVP and G7500 had less scatter in the flexural strength, as reflected in their higher Weibull moduli of 11.9 and 10.2, respectively. The Weibull modulus is a good measure for the influence of sintering and processing techniques on materials properties and the reliability of the final parts, and these relatively high values for ceramic materials indicates a more reliable process. The values reported here are similar to the >10 Weibull modulus values expected for commercial pressureless sintered Si_3N_4 materials [44], as well as to other colloidal and near-net processing of Si_3N_4 studies that have reported Weibull modulus values from 4 to 15 [45–48].

The Weibull distribution assumes a single population of defect types; in this study the primary defect is assumed to be the porosity observed on the fracture surface of the bend bars (values reported in Table 2), as it is the largest scale change observed in the sample sets. The pore size on the fracture surface cross-section represents the size scale of the porosity causing failure, and it is assumed to be representative of the porosity throughout the specimen volume. An example of an optical image of a G7500-PVP bend bar fracture surface used for pore size analysis is shown in Fig. 8. The flexural strength is plotted as a function of this pore size in Fig. 9 showing a clear and expected trend where samples with smallest average pore size (A575-PVP and G7500) have the largest average flexural strength. The estimated flexural strength for a pore free specimen is 857.5 MPa, calculated as the y-intercept of a polynomial fit to this data (R^2 > 0.99). This is similar to the high end of the reported flexural strengths for pressureless sintered Si_3N_4 [27,28,39–41,43,44].

The estimated average fracture toughness for each suspension set is listed in Table 2 and was calculated using the equation in Section 2.4 with the measured average pore size set equal to two times the crack size (c). The average fracture toughness in this study range from 3.76 to 4.70 MPa $m^{0.5}$, within the reported range for Si_3N_4 of 3–12 MPa $m^{0.5}$ [43,49]. The wide reported range for Si_3N_4 is due to both changes in microstructure (mainly grain size, orientation, and aspect ratio as well as intergranular glass amount and composition) and method for determining fracture toughness [49].

The high standard deviation in pore size for G7500-PVP and A575,

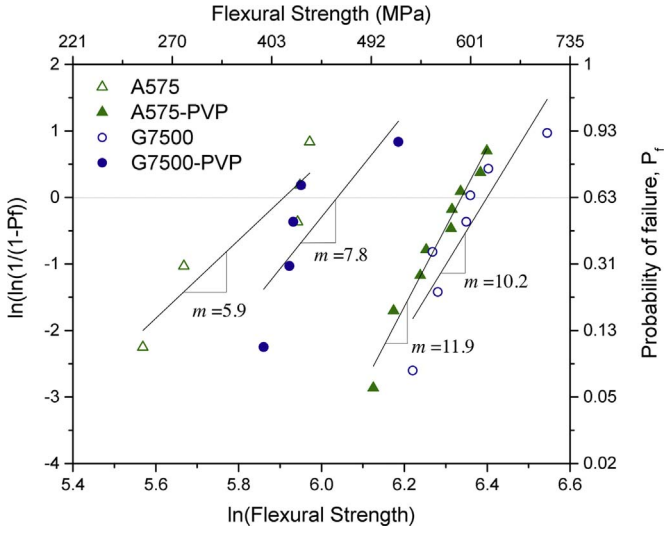

Fig. 7. Weibull plots of the flexural strength of Si_3N_4 specimens made via injection molding four different aqueous suspensions.

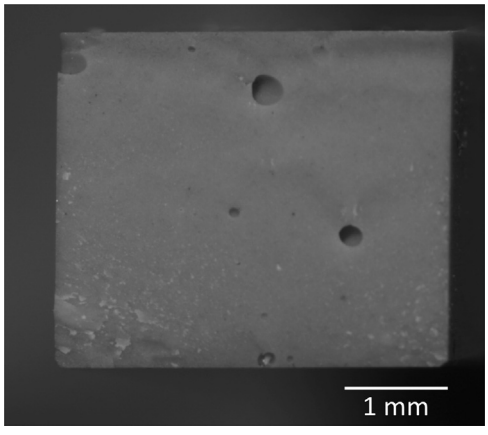

Fig. 8. A representative optical image of a bend bar fracture surface (tensile edge on the bottom of image) of a G7500-PVP specimen with porosity present from processing. ImageJ was used to manually calculate the average pore size for each specimen.

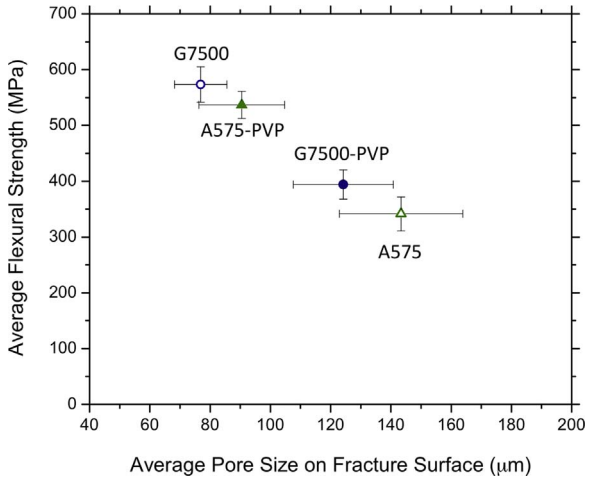

Fig. 9. The average flexural strength as a function of average pore size on the fracture surface for all four suspensions used in the injection molding experiments. The measured porosity is from forming rather than incomplete sintering.

and their corresponding lower Weibull moduli, suggest these suspensions created more variable and larger porosity during forming. On the other hand, A575-PVP and G7500 had less variability in measured pore size, and therefore high Weibull moduli, which implies greater reliability for ceramic processing.

Due to the size scale of the porosity, and the evidence of near complete sintering from microstructure analysis, it is clear that most of the porosity is introduced during the forming process during one, or a combination, of the following steps: 1) suspension mixing, 2) syringe filling and mixing, and 3) injection molding. To determine if air was entrapped in the suspension during steps 1 and 2, a batch of all four suspensions was produced using the mixing cycle outlined in Section 2.1. Half of the suspension was left in the mixing container to dry while the other half was added to a syringe and mixed using the parameters listed in Section 2.2. The suspension was dried out over a period of three days to examine the porosity in the dried green state. Optical analysis of both the dried suspension in the mixing container and the suspension dried in the syringe revealed porosity on the same size scale of the measured porosity on the sintered fracture surfaces. Therefore, air was entrapped during mixing, syringe filling, or a combination of both processes (rather than during injection molding), which lead to porosity in the final sintered specimens.

The commercial comb-polymers used as dispersants in this study are typically used in concrete mixtures in order to decrease the water-to-cement ratio, hence the commercial title of water reducing admixtures (WRAs) [50]. Unfortunately, common commercial WRAs have been found to exhibit high foaming action during the mixing of concrete which causes a high air content and subsequent decrease in mechanical strength [50]. This foaming action has been tied to the presence of an appreciable amount of unreacted macromonomer (~10 wt%) in the commercial WRA aqueous solutions [50]. These macromonomers can interact with the solid-liquid-air interfaces to stabilize the air bubbles within the suspension, as seen in concrete mixtures [51]. The mass of the ceramic particles or agglomerates has also been reported to help to disperse air bubbles in the mixture to reduce their tendency to float to the surface [51]. In addition, the yield stress of the suspensions aids to entrap the air bubbles that are introduced during mixing if their buoyancy forces (as determined by the viscosity of the suspension and the size of the bubble) are not large enough to escape [51].

Low viscosity fluids provide little barrier to air bubble coalescence, [51] which could explain the larger porosity observed in the sintered specimens made from the suspension with the lowest viscosity (A575). The low viscosity of A575 may also indicate a high level of entrapped air in the suspension, which has been shown to lower the viscosity of cement mixtures [51]. With the addition of PVP to the A575 suspension, a statistically significant decrease in average porosity size on the sintered fracture surface (listed in Table 2) is observed, possibly due to the higher energy barrier for coalescence of the bubbles in the higher viscosity A575-PVP suspension. The suspensions made with Glenium 7500 have a higher viscosity at rest (near 0 s^{-1}), such that they may resist bubble coalescence, but high enough that they can overpower the buoyancy forces needed for the air bubbles to escape. A study on varied mixing times and lengths, as well as the addition of a vacuum during mixing, would be helpful to minimize the size and amount of air entrapped. The types of fatty alcohols that have been employed in both the concrete and ceramic processing fields as a defoaming agent can also be explored to further reduced entrapped air [50,52].

It is unclear if additional porosity is introduced during injection molding, but since air is allowed to escape the mold through the air vents highlighted in Fig. 1, it is estimated that no additional large-scale porosity is being introduced through this step. Regardless, the overall porosity could be minimized through removal of the entrapped air during mixing and syringe filling. Minimizing entrapped air in the suspensions should help increase both average flexural strength and Weibull modulus through a reduction in the amount and size of the porosity in the sintered specimens.

4. Conclusions

A novel low-pressure and room-temperature injection molding process was successfully created to produce robust Si_3N_4 parts using highly-loaded (45 vol%) aqueous suspensions that were free of harsh chemicals or cross-linking agents. The low amount of polymer dispersant and binder allowed the use of short binder burnout cycles, which led to specimens with no visual cracking or warpage defects. Four suspension sample sets were examined, with all leading to high average sintered densities over 94%TD after pressureless sintering. Of the four suspensions studied, A575-PVP and G7500 were identified as optimal due to specimens with the smallest average porosity (< 100 μm) measured from the fracture surface, highest average flexural strength (540–570 MPa), and highest Weibull modulus 10–12). Air was entrapped in the suspension during mixing and syringe filling, likely due to the foaming behavior of the commercial comb-polymers used as a dispersant for the ceramic suspensions. This entrapped air lead to porosity in the sintered part, which can be removed in future studies through mixing improvements or the addition of defoaming agents to further increase the mechanical behavior. The robust mechanical properties, even with the porosity present, prove this to be a viable process for making Si_3N_4 parts. This novel injection molding process is easily scalable due to the low-pressure and economical tooling used, and could expand the use of Si_3N_4 due to the ability to create near-net and complex shapes.

Acknowledgements

This work was supported by the Army Research Office [Grant W911NF-13-1-042] and the National Science Foundation [Graduate Research Fellowship Program, Grant DGE-1333468]. The authors are also grateful to Professor Kendra Erk for insightful discussions and Professor Carlos Martinez for helpful discussions and for the rheometer training and use.

References

[1] F.L. Riley, Silicon nitride and related materials, J. Am. Ceram. Soc. 83 (2000) 245–265.
[2] R.W. Trice, J.W. Halloran, Mode I fracture toughness of a small-grained silicon nitride: orientation, temperature, and crack length effects, J. Am. Ceram. Soc. 82 (1999) 2633–2640.
[3] S. Hampshire, Silicon nitride ceramics – review of structure, processing and properties, J. Achiev. Mater. Manuf. Eng. 24 (2007) 43–50.

[4] S. Hampshire, M.J. Pomeroy, Grain boundary glasses in silicon nitride: a review of chemistry, properties and crystallisation, J. Eur. Ceram. Soc. 32 (2012) 1925–1932.
[5] X. Zhu, Y. Sakka, Textured silicon nitride: processing and anisotropic properties, Sci. Technol. Adv. Mater. 9 (2008) 33001.
[6] M.K. Ferber, M.G. Jenkins, Evaluation of the strength and creep-fatigue behavior of hot isostatically pressed silicon nitride, J. Am. Ceram. Soc. 75 (1992) 2453–2462.
[7] B. Bhushan, L.B. Sibley, Silicon nitride rolling bearings for extreme operating conditions, A S L E Trans. 25 (2008) 417–428.
[8] B. Wang, J. Yang, R. Guo, J. Gao, J. Yang, Microstructure and property enhancement of silicon nitride-barium aluminum silicate composites with β-Si3N4 seed addition, J. Mater. Sci. 44 (2008) 1351–1356.
[9] W.M. Sigmund, N.S. Bell, L. Bergstrom, Novel powder-processing methods for advanced ceramics, J. Am. Ceram. Soc. 83 (2000) 1557–1574.
[10] J. Lenz, R.K. Enneti, S.-J. Park, S.V. Atre, Powder injection molding process design for UAV engine components using nanoscale silicon nitride powders, Ceram. Int. 40 (2014) 893–900.
[11] B.C. Mutsuddy, R.G. Ford, Ceramic Injection Molding, 1st ed., Chapman & Hall, London, 1995.
[12] M.J. Edirisinghe, J.R.G. Evans, Review: fabrication of engineering ceramics by injection moulding. I. Materials selection, Int. J. High. Technol. Ceram. 2 (1986) 1–31.
[13] J. Woodthorpe, M.J. Edirisinghe, J.R.G. Evans, Properties of ceramic injection moulding formulations. Part 3 Polymer Removal, J. Mater. Sci. 24 (1989) 1038–1048.
[14] S. Leo, C. Tallon, N. Stone, G.V. Franks, Near-net-shaping methods for ceramic elements of (body) armor systems, J. Am. Ceram. Soc. 97 (2014) 3013–3033.
[15] A.J. Millan, M. Nieto, R. Moreno, Aqueous injection moulding of silicon nitride, J. Eur. Ceram. Soc. 20 (2000) 2661–2666.
[16] L.M. Rueschhoff, J.P. Youngblood, R.W. Trice, Stabilizing highly loaded silicon nitride aqueous suspensions using comb polymer concrete superplasticizers, J. Am. Ceram. Soc. 99 (2016) 3857–3865.
[17] J. Yang, T. Ohji, Influence of Yttria – alumina content on sintering behavior and microstructure of silicon nitride ceramics, J. Am. Ceram. Soc. 83 (2000) 2094–2096.
[18] O. Abe, Sintering process of Y_2O_3 and Al_2O_3-doped Si_3N_4, J. Mater. Sci. 25 (1990) 4018–4026.
[19] D. Suttor, G.S. Fischman, Densification and sintering kinetics in sintered silicon nitride, J. Am. Ceram. Soc. 75 (1992) 1063–1067.
[20] D. Lee, S.L. Kang, G. Petzow, D.N. Yoon, Effect of α to β (β') Phase Transformation on the Sintering of Silicon Nitride Ceramics, J. Am. Ceram. Soc. 73 (1990) 767–769.
[21] T. Honma, Y. Ukyo, Sintering process of Si_3N_4 with Y_2O_3 and Al_2O_3 as sintering additives, J. Mater. Sci. Lett. 8 (1999) 735–737.
[22] W.J. Tseng, Influence of surfactant on rheological behaviors of injection–molded alumina suspensions, Mater. Sci. Eng. A. 289 (2000) 116–122.
[23] J.H. Song, J.R.G. Evans, Ultrafine ceramic powder injection moulding: the role of dispersants, J. Rheol. (N. Y. N. Y). 40 (1996) 131.
[24] W. Herschel, R. Bulkley, Consistency of Measurements in Rubber-Benzene Solutions, Colloid J. 39 (1926) 291–300.
[25] T.F. Tadros, Rheology of Dispersions: Principles and Applications, 1st ed., Wiley-VCH Verlag GmbH & Co. KGaA, Weinheim, Germany, 2010.
[26] M.J. Edirisinghe, M.S. Heidi, K.L. Tomkins, Flow behaviour of ceramic injection moulding suspensions, Ceram. Int. 18 (1992) 193–200.
[27] Z. Huang, A. Rosenflanz, I. Chen, Pressureless sintering of Si3N4 ceramic using AlN and rare-earth oxides, J. Am. Ceram. Soc. 80 (1997) 1256–1262.
[28] W. Zeng, X. Gan, Z. Li, K. Zhou, The preparation of silicon nitride ceramics by gelcasting and pressureless sintering, Ceram. Int. 42 (2016) 11593–11597.
[29] S. Hampshire, Silicon nitride ceramics, Mater. Sci. Forum 606 (2009) 27–41.
[30] S. Hampshire, Nitride ceramics, in: R.W. Cahn, P. Haasen, E.J. Kramer (Eds.), , Mater. Sci. Technol. A Compr. Treat. 11, VCH, 1993, pp. 119–172.
[31] M.W. Barsoum, Fundamentals of Ceramics, Taylor & Francis Group, LLC, 2003.
[32] J.C. Newman, I.S. Raju, An empirical stress-intensity factor equation for the surface crack, Eng. Fract. Mech. 15 (1981) 185–192.
[33] J.E. Smay, J. Cesarano, J.A. Lewis, Colloidal Inks for Directed Assembly of 3-D Periodic Structures, Langmuir 84 (2002) 5429–5437.
[34] M. Acosta, V.L. Wiesner, C.J. Martinez, R.W. Trice, J.P. Youngblood, Effect of Polyvinylpyrrolidone Additions on the Rheology of Aqueous, Highly Loaded Alumina Suspensions, J. Am. Ceram. Soc. 96 (2013) 1372–1382.
[35] V.L. Wiesner, J.P. Youngblood, R.W. Trice, Room-temperature injection molding of aqueous alumina-polyvinylpyrrolidone suspensions, J. Eur. Ceram. Soc. 34 (2014) 453–463.
[36] R.L. Hoffman, Explanations for the cause of shear thickening in concentrated colloidal suspensions, J. Rheol. (N. Y. N. Y). 42 (1998) 111–123.
[37] P. Thomas-Vielma, A. Cervera, B. Levenfeld, A. Várez, Production of alumina parts by powder injection molding with a binder system based on high density polyethylene, J. Eur. Ceram. Soc. 28 (2008) 763–771.
[38] R.E. Loehman, D.J. Rowcliffe, Sintering of Si_3N_4-Y_2O_3-Al_2O_3, J. Am. Ceram. Soc. 63 (1976) 144–148.
[39] T. Quadir, A. Arfaei, Aqeous Extrus. Silicon Nitride 5 (209) (1993) 885.
[40] O. Penas, R. Zenati, J. Dubois, G. Fantozzi, Processing, microstructure, mechanical properties of Si3N4 obtained by slip casting and pressureless sintering, Ceram. Int. 27 (2001) 591–596.
[41] J. Yang, F.J. Oliveira, R.F. Silva, J.M.F. Ferreira, Pressureless sinterability of slip cast silicon nitride bodies prepared from coprecipitation-coated powders, J. Eur. Ceram. Soc. 19 (1999) 433–439.
[42] G. He, D.A. Hirschfeld, J. Cesarano III, J.N. Stuecker, Process. Silicon Nitride Ceram. Conc. Aqueous Suspens. Rob. (2000) 1–12.
[43] G. Ziegler, J. Heinrich, G. Wotting, Review: relationships between processing, microstructure and properties of dense and reaction-bonded silicon nitride, J. Mater. Sci. 22 (1987) 3041–3086.
[44] H. Lange, G. Wotting, G. Winter, Silicon Nitride-From Powder Synthesis to Ceramic Materials, Agnew. Chem. Int. Ed. Engl. 30 (1991) 1579–1597.
[45] S. Iyer, J. Mcintosh, A. Bandyopadhyay, N. Langrana, A. Safari, S.C. Danforth, Microstructural Characterization and Mechanical Properties of Si_3N_4 Formed by Fused Deposition of Ceramics, Int. J. Appl. Ceram. Technol. 5 (2008) 127–137.
[46] O.O. Omatete, M.A. Janney, S.D. Nunn, Gelcasting: from laboratory development toward industrial production, J. Eur. Ceram. Soc. 17 (1997) 407–413.
[47] Y. Huang, L. Zhou, Q. Tang, Z. Xie, J. Yang, Water-Based Gelcasting of Surface-Coated Silicon Nitride Powder, J. Am. Ceram. Soc. 84 (2001) 701–707.
[48] Y. Huang, L. Ma, Q. Tang, J. Yang, Z. Xie, X. Xu, Surface oxidation to improve water-based gelcasting of silicon nitride, J. Mater. Sci. 35 (2000) 3519–3524.
[49] G. Petzow, M. Herrmann, Silicon Nitride Ceramics, in: M. Jansen (Ed.)High Perform. Non-Oxide Ceram. II, Springer, 2002, pp. 47–167.
[50] A. Lange, J. Plank, Study on the foaming behaviour of allyl ether-based poly-carboxylate superplasticizers, Cem. Concr. Res. 42 (2012) 484–489.
[51] L. Du, K.J. Folliard, Mechanisms of air entrainment in concrete, Cem. Concr. Res. 35 (2005) 1463–1471.
[52] B. Bitterlich, J.G. Heinrich, Aqueous tape casting of silicon nitride, J. Eur. Ceram. Soc. 22 (2002) 2427–2434.